USING OPTICAL IMAGERY DATA FOR LITHOLOGICAL MAPPING OF COMPOSITE VOLCANOES IN HIGH ARID PUNA PLATEAU. TUZGLE VOLCANO CASE STUDY

Emilce BUSTOS[1], Walter A. BÁEZ[1], Gianluca NORINI[2], Agostina L. CHIODI[1], Gianluca GROPPELLI[2] and José M. ARNOSIO[1]

[1] GEONORTE - INENCO (Universidad Nacional de Salta - CONICET), Salta. Email: emilcebustos@gmail.com
[2] Istituto per la Dinamicadei Processi Ambientali, Consiglio Nazionale delle Ricerche, Italia.

ABSTRACT

Geological mapping of volcanic areas is important to unravel the evolution of the volcanism with significant implication for the assessment of the geologic hazard and the exploration and exploitation of energy and mineral resources. Volcanic mapping in Puna plateau is a challenging task due to inaccessibility, extreme climatic conditions, high altitude above sea level and dangerous issues like minefields, so an effective and validated methodology for mapping is fundamental to ensure the quality of the final results for the end-users. A practical mapping methodology using optical imagery data is tested in Cerro Tuzgle because of its well-known stratigraphy is presented. Some of the most common and well known processing techniques (false color combinations, band ratios and principal component analysis) were used to multispectral data (Landsat 7, Landsat 8 and ASTER). Then, supervised classification and an assessment of the classification were produced for every image created. The quantitative accuracy of the classification maps resulting from different data sets was assessed by comparing the classification with ground truth data extracted from the geological map by means of a confusion matrix and related statistics. Since the validation over several processing techniques, we found that supervised classification over principal component analysis in multispectral data was the best methodology for lithological mapping in volcanic areas. Comparing the three multispectral sensors used in this work, we achieve better results and more accuracy with ASTER images. Low costs, data availability and broad swath of the multispectral data make these images valuable for lithological mapping in arid volcanic regions. This time- and cost-effective methodology is adequate to composite volcano preliminary mapping, but the correct reconstruction of the stratigraphy of a volcano always requires field survey.

Keywords: *Volcanic mapping, Optical remote sensing, Tuzgle volcano, Puna plateau, Geological map*

RESUMEN

Mapeo litológico de volcanes compuestos en el plateau de la Puna usando datos satelitales ópticos: caso de estudio volcán Tuzgle
El mapeo de zonas volcánicas es importante para revelar la evolución del volcanismo con importantes implicancias en la evaluación del riesgo geológico y en la exploración y explotación de recursos minerales y energéticos. El mapeo volcánico en la región la Puna es una tarea que implica un desafío importante debido a la inaccesibilidad, condiciones climáticas extremas, la elevada altitud sobre el nivel del mar y problemas peligrosos como los campos minados. Por estas razones una metodología efectiva para el mapeo es muy importante. En esta contribución se presenta una técnica práctica de mapeo usando imágenes satelitales ópticas usando como zona piloto al cerro Tuzgle ya que éste cuenta con estudios estratigráficos de detalle fundamentales para validar los resultados. Se obtuvieron imágenes utilizando técnicas de procesamiento (combinaciones falso color, cocientes de bandas, análisis de componentes principales) comunes y conocidas sobre imágenes ópticas multiespectrales (Landsat 7, Landsat 8 y ASTER). Luego, las imágenes fueron clasificadas y su exactitud se evaluó por medio de matrices de confusión y estadísticos, mediante la comparación de los resultados de la clasificación con la verdad de campo extraída del mapa geológico. La clasificación supervisada sobre imágenes derivadas del análisis de componentes principales fue la mejor metodología para el mapeo litológico. Por otro lado, la comparación entre los sensores multiespectrales mostró que la mayor exactitud se obtuvo con los datos ASTER. El bajo costo, la disponibilidad de datos y la amplia cobertura de los datos multiespectrales son características que hacen a estos productos muy apropiados para el mapeo litológico en regiones volcánicas áridas. Aunque esta metodología es efectiva para el mapeo preliminar de volcanes compuestos, la definición estratigráfica correcta de un volcán siempre requiere relevamiento de campo.

Palabras clave: *Mapeo volcánico, Sensores remotos ópticos, Volcán Tuzgle, Plateau de la Puna, Mapa geológico*

INTRODUCTION

Detailed geological mapping of volcanic areas is relevant to determine the rock types that have been erupted, their spatial distribution and stratigraphic relationships. These determinations may enable to unravel the characteristics and evolution of the volcanism in an area, with im-

portant implication for the assessment of the geologic hazard and the exploration and exploitation of energy and mineral resources.

The use of remote sensing data for geological mapping has been recently increased due to the high spatial and spectral resolution of current satellite images. Moreover, the improvement of methodologies and techniques of remote sensing and data analysis, and the worldwide availability of these data – often as open access data- make the use of satellite images for geological mapping feasible. Visible and near/shortwave-infrared optical remote sensing is a primary tool for geological mapping, providing a wealth of information on the composition, mineralogy and morphology of Earth´s surface (*e.g.* van der Meer *et al.* 2012). Also, lithological identification and silica content can be performed using multispectral thermal infrared data (*e.g.* Ninomiya and Fu 2002, Watanabe and Matsuo 2003, Moghtaderi *et al.* 2007, Aboelkhair *et al.* 2010). Popular techniques for hydrothermal characterization and geological mapping on multispectral data are, for example, color band compositions (*e.g.* Assiri *et al.* 2008, Qary *et al.* 2008), band ratios (*e.g.* Abrams *et al.* 1983, Abdelsalam and Stern 1996, Rowan and Mars 2003, Rowan *et al.* 2003, Di Tommaso and Rubinstein, 2007) and principal component analysis (*e.g.* Crosta and Moore 1989, Gomez *et al.* 2005, Tangestani 2006, Amer *et al.* 2010). Remote sensing data are particularly suitable for the geological mapping of difficult to access or inaccessible or large non-vegetated areas. In these cases an effective and validated methodology is fundamental to ensure the quality of the final results for the end-users.

One of the most suitable volcanic areas for geological mapping with remote sensing data is the Altiplano-Puna plateau of the Central Andes, the second highest plateau in the world, associated with abundant arc magmatism related to subduction (de Silva and Francis 1991, Allmendinger *et al.* 1997, Trumbull *et al.* 2006). Field geological mapping of this area is a challenging task due to inaccessibility, extreme climatic conditions, high altitude above sea level and dangerous issues like minefields. On the other hand, this region has appropriate conditions for the application of remote sensing mapping techniques like high altitude (4.000 m a.s.l.), allowing few atmosphere errors; arid climate, making the vegetal cover almost null; and extensive outcropping areas, exposing a wide range of different volcanic and non-volcanic rock types.

In this paper we present a practical mapping methodology for arid volcanic regions using optical imagery data, that has been tested in the area of the Cerro Tuzgle, a Quaternary composite volcano (24°S 66,5°W) located in the central Puna Plateau, in the Jujuy Province, NW Argentina. A comparative approach between multispectral (Landsat ETM+- Enhanced Thematic Mapper Plus, Landsat 8 and ASTER- Advanced Spaceborne Thermal Emission and Reflection Radiometer) data is proposed, in order to evaluate their advantages for lithological mapping in volcanic areas. This study aims to find a practical and efficient method using optical images in arid regions for the preliminary mapping of volcanic areas. The principal objective is to find the better combination of accuracy and reproducibility among the remote sensing analysis results in comparison with the ground truth data. The Cerro Tuzgle volcano was used as a pilot area since it is one of the few volcanic centers of the Puna region with a well-known ground-truth stratigraphic data (Coira and Kay 1993, Cogliati 2011, Norini *et al.* 2014). Moreover, cerroTuzgle has a huge compositional/textural and spectral variation, from riodacites to basaltic andesites, and from effusive to explosive and epiclastic products.

GEOLOGICAL SETTING

Volcanism in the Cenozoic Andean Cordillera is generated by the subduction of the Nazca and Antarctica plates beneath the South American plate. In the Central Andes, Miocene-Quaternary volcanic activity occurred within the Central Volcanic Zone (Deruelle 1982) in two well-defined segments: the Western Cordillera magmatic arc and the Altiplano-Puna Plateau back-arc region. The volcanic activity in the Puna Plateau comprises composite volcanoes, calderas and monogenetic centers, which has been associated with NW-SE strike-slip faults and N-S orogen-parallel thrust faults (*e.g.* Allmendinger *et al.* 1983, Viramonte *et al.* 1984, Viramonte and Petrinovic 1990, Yuan *et al.* 2000, Riller *et al.* 2001, Matteini *et al.* 2002, ANCORP Working Group 2003, Petrinovic *et al.* 2006, Trumbull *et al.* 2006, Kay and Coira 2009, Acocella *et al.* 2011, Norini *et al.* 2013).

One of the youngest and best exposed polygenetic volcanic centers of the Puna Plateau is the Cerro Tuzgle volcano. This stratovolcano has been associated, together with numerous Miocene to Recent volcanoes, to the active left-lateral strike-slip Calama-Olacapato-El Toro fault system (Fig. 1) (*e.g.* Allmendinger *et al.* 1983, Salfity 1985, Viramonte *et al.* 1984, Matteini *et al.* 2002, Petrinovic *et al.* 2006, Ramelow *et al.* 2006, Mazzuoli *et al.* 2008, Acocella *et al.* 2011, Norini *et al.* 2013).

Cerro Tuzgle stratovolcano (0.65 My-Holocene?, Schwab and Lippolt 1976, de Silva and Francis 1991, González-Ferrán 1995) is the largest and largely geochemical varying Quaternary center in the back-arc region of the Central Volcanic Zone (Coira and Kay 1993). Petrologic and geochemical data show that Cerro Tuzgle is a high-K calcalkaline andesitic-rhyodacitic volcanic center with complex mixtures of crustal and mantle-derived components (Coira and Kay 1993). This volcanic center is positioned about 280 km behind the active magmatic arc and is situated in an N-S-trending, thrust fault-bounded, intramontane depression. This tectonic depression is closed southward by the Calama-Olacapato-El Toro fault scarps and has a northward gently dipping floor.

Norini *et al.* (2014) present a detailed 1:25,000 geological map of the Tuzgle Volcano and its stratigraphic reconstruction, based on the main unconformities (synthemic units) (Fig. 2). These uncon-

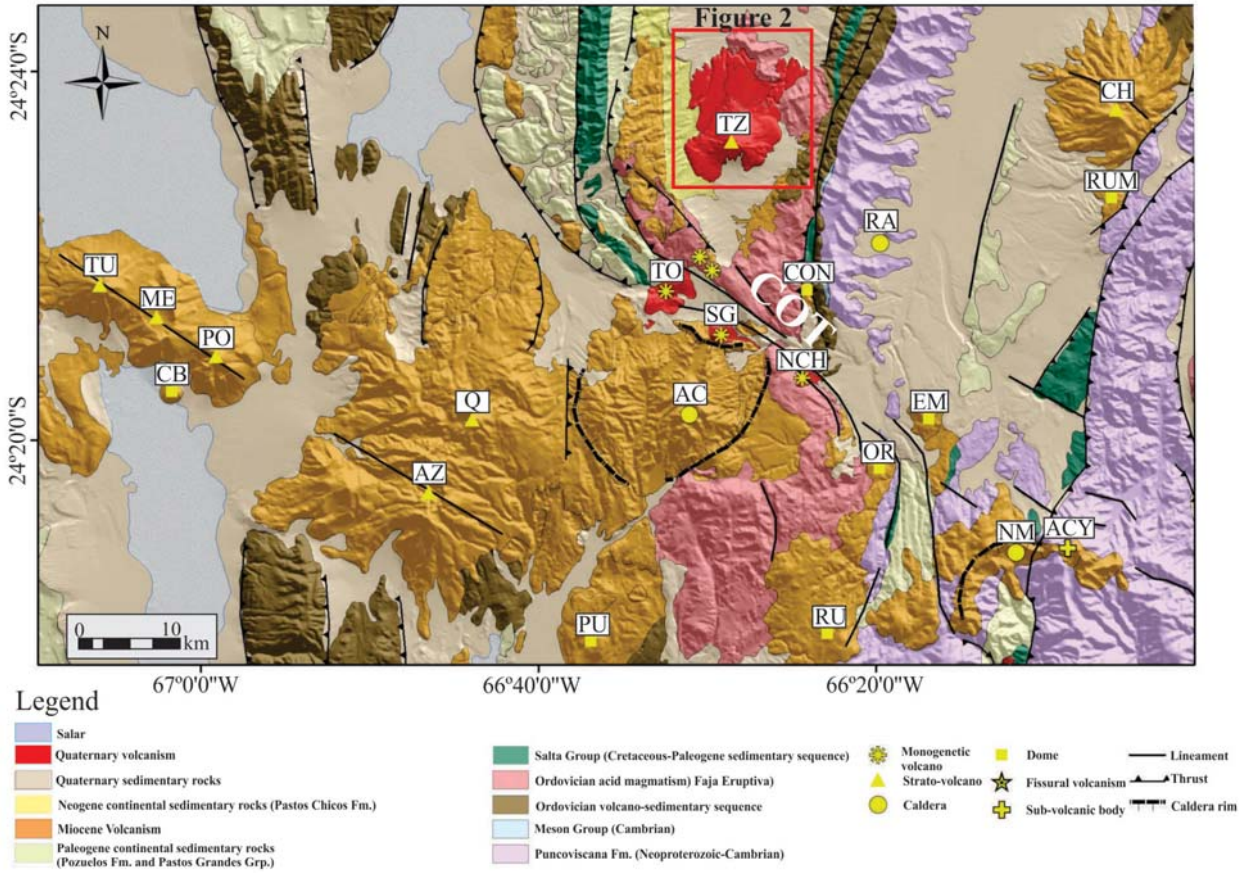

Figure 1: Regional geological map of the back-arc Puna Plateau in the Cerro Tuzgle area on a SRTM shadow relief. TU: Tul Tul; ME: Del Medio; PO: Pocitos; CB: Cerro Bola; AZ: El Azufre; Q: Quevar; PU: Pucara; RU: Rupasca; AC: Aguas Calientes; OR: Organullo; NCH: Negro del Chorrillo; SG: San Geronimo; TO: Tocomar; TZ: Tuzgle; CON: Concordia; RA: Ramada; EM: El Morro; NM: Negra Muerta; ACY: Nevado de Acay; CH: Chimpa; RUM: Rumio; COT: Calama–Olacapato–El Toro FaultSystem. After Norini *et al.* (2014). The location of figure 2 is shown.

formity surfaces at the volcano scale are related to angular and/or erosional unconformities, significant changes in the eruptive style, shiftings in the feeding system and/or volcano tectonic events. The Quaternary volcanic activity in the area of Cerro Tuzgle started with an ignimbritic eruption (Tuzgle Ignimbrite synthem), followed by the emplacement of scattered lava domes (Basal Dome Complex synthem) and the construction of a central volcano (San Antonio, Azufre and Tuzgle synthems), which generated at least one northward sector collapse. The evolution of the Cerro Tuzgle stratovolcano and the resulting volcanic products are described in the Table 1.

SATELLITARYDATA

Landsat 7 ETM+, Landsat 8 and ASTER multispectral imagery were used for the geological mapping of Cerro Tuzgle volcano (Fig. 3). These images were chosen because of their wide diffusion, availability, free cost and quality. Landsat 7 image is an orthorectified scene downloaded from the Global Land Cover Facility acquired on March 11, 2000 at 14:15:25 UTC. Landsat 8 image was acquired on February 19, 2014 at 14:25:54 UTC. ASTER data correspond to February 17, 2007, at 14:27:02 UTC. The scenes correspond to the path 232 and row 077. The Landsat 8 and ASTER data are courtesy of the US Geological Survey.

Landsat 7 was launched in 1999. It is equipped with ETM+ sensor and has 8 wavelength bands: 3 visible, 1 near-infrared and 2 short-wave infrared (SWIR) bands (30 m spatial resolution), 1 thermal IR (TIR) band (60 m spatial resolution) and 1 panchromatic band (15 m spatial resolution) (Fig. 3). Landsat 8 was launched on February 2014 and it has two Earth observing sensors, the Operational Land Imager (OLI) and the Thermal Infrared Sensor (TIRS) (Roy *et al.* 2014). The sensors include nine spectral bands with a spatial resolution of 30 meters (Band 1 to 7 and 9, Fig. 3). Landsat 7 and 8 scenes cover a 170 km x 185 km land area. ASTER (Yamaguchi *et al.* 1998) was launched in 1999 collects data in 14 bands, three in the visible and near-infrared (VNIR, 15 m spatial resolution), six in the short-wave infrared (SWIR, 30 m spatial resolution) and five in the thermal infrared (TIR, 90 m spatial resolution) (Fig. 3). An additional capability offered by ASTER is the stereoscopic acquisition in a VNIR band. The ASTER imagery provides scene coverage of 60 x 60 km.

VNIR bands are useful for identifying vegetation, iron-oxide minerals and mapping gossans (Papp and Cudahy

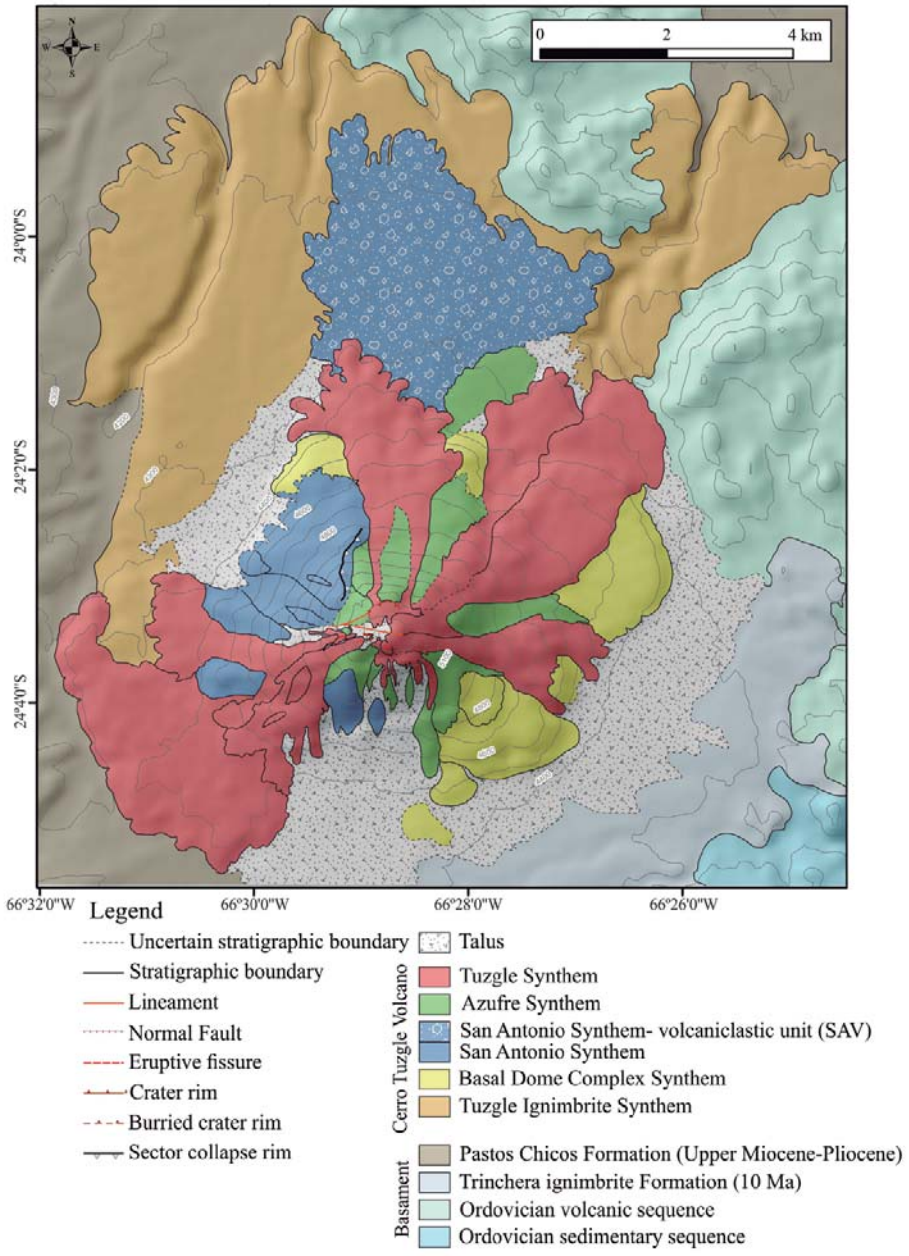

Figure 2: Geological map of the Cerro Tuzgle volcano. After Norini *et al.* (2014).

2002), since mineral spectral features in this wavelength region are related to the charge transfer effect of electrons between energy levels of constituent elements especially the transitional metals, Fe, Mn, and Cr (Hunt *et al.* 1971). On the other hand, the SWIR bands are functional for alteration mineral mapping (*e.g.* Hubbard *et al.* 2003, Rowan *et al.* 2003). The mineral spectral features in the SWIR are largely related to the overtones and combination tones of vibrationals of octahedrally coordinated cations (typically, Al, Fe, Mg) bonded with OH groups (Hunt and Vincent 1968). Mineral spectral features in the TIR wavelength region are related to vibrations of Si-O bonds (Lyon 1965). TIR data allow characterizing features exhibited by rock-forming mineral groups such as silicates and carbonates, therefore is useful for mapping lithologies and rock-forming minerals (*e.g.* Jensen 2002, Papp and Cudahy 2002, Gutpa 2003).

METHODOLOGY

The purpose of this study was to develop a practical and efficient preliminary mapping method for volcanic areas using optical satellite data with simple and fast known techniques. The research procedure for this study is shown in the flow diagram of figure 4.

Landsat 7, 8 and ASTER data are used as input, in order to evaluate their advantages for lithological mapping in Tuzgle volcanic area. The first step was choosing cloud free images, and then, preprocessing was applied (for pre-processing details see: Fernandes *et al.* 2004 for Landsat 7, Bhatti and Tripathi 2014 for Landsat 8, and Son *et al.* 2014 for ASTER data). Optical data pre-processing included radiometric and geometric corrections. Pre-processing of ASTER data also incorporated Crosstalk correction. The atmospheric correction was not performed because the atmosphere of the study area is dry and clean and because it is beyond the scope of this work. Over these data the most common and well known processing techniques (listed in Table 2) were used. These techniques are false color composite images, band ratio images and Principal Component Analysis.Color composite images are visualized by assigning three bands to a color space defined by red, green and blue values. Band Ratios were applied since they enhance compositional variation reducing differences due to the effects of albedo and topographic slope. This methodology is effective in emphasizing spectral characteristics of certain rocks and minerals (*e.g.* Abdeen *et al.* 2001, Velosky *et al.* 2003, Rowan and Mars 2003, Rowan *et al.* 2003).Principal component analysis is used to produce uncorrelated output bands, to segregate noise components, and to reduce the dimensionality of data sets (*e.g.* Gomez *et al.* 2005, Tangestani 2006, Amer *et al.* 2010). Several images were generated and here the images with best results were shown.

Over each processing product (listed in Table 2), equal homogeneous and representative surfaces named training regions (training data or end-members)

TABLE 1: Description of Tuzgle Volcano synthems.

Synthem	Boundary	Unconformity	Eruptive Style/ Products	Composition
Tuzgle Ignimbrite	Lower Upper	Non conformity with Faja Eruptiva and Pastos Chicos Formation. Angular unconformity with the overlying lithostratigraphic units associated with an eruptive style change	Ignimbritic deposits, associated with the formation of a caldera depression, not identified during field work; it represents the first deposit associated with the beginning of a new eruptive cycle.	Porphyritic texture. P.I. 10% (pumice) Phenocrystals of plagioclase, quartz, biotite, sanidine, orthopiroxene, zircon and oxides. Rhyodacitic. Porphyritic texture. P.I. 25-35%.
Basal Dome Complex	Upper	Angular unconformity with the overlying lithostratigraphic units associated with an eruptive style change.	Medium grained crystal rich lavas which form high, circular and flat-topped hills with steep flanks, interpreted as dacitic domes. They represent the first magmatic constructive event of the volcanic edifice.	Phenocrystals of plagioclase, biotite, quartz, clinopyroxene, orthopyroxene, zircon and oxides. Dacitic.
San Antonio	Upper	Sharp angular unconformity due to a volcano-tectonic event (lateral collapse)	Crystal rich lava flows that form rounded and elongated humps. Dacitic-andesitic lavas represent the second constructive event of the volcanic edifice.	Porphyritic texture. P.I. 15-35%. Phenocrystals of plagioclase, biotite, quartz, orthopyroxene, clinopyroxene, Ti-amphibole, zircon and oxides. Dacitic-andesitic.
Azufre	Upper	Angular unconformity due to the NE-SW elongated rim crater, called platform, probably linked to a volcano-tectonic event.	Crystal rich lava flows. Effusive volcanic activity occurred after the volcano-tectonic event (lateral collapse). HydrothermalAltered.	Porphyritic texture. P.I. 25-35%. Phenocrystals of plagioclase, biotite, quartz, Ti-amphibole, orthopyroxene, clinopyroxene, zircon and oxides. Andesitic-dacitic.
Tuzgle	Upper	Present topography.	Lava flows reaching the base of the volcano forming steep flanks and linear or lobate fronts. Andesitic blocky lavas represent the last phase of the eruptive history of the Tuzgle Volcano.	Porphyritic texture. P.I. 25-35%. Phenocrystals of plagioclase, quartz, Ti-amphibole, orthopyroxene, clinopyroxene and olivine. Andesitic.

TABLE 2: Processing techniques. Classification accuracy and Kappa coefficient. Overall accuracy* values are also presented after joint Tuzgle Ignimbrite and Basal Dome.

Image	Processing RGB	Reference	Overallaccuracy (%)	Kappa coefficient	Overallaccuracy* (%)
Landsat 7	5/3 5/1 7/5	Gad and Kusky (2006)	42.38	0.2987	54.86
	7/5 5/4 3/1	Gad and Kusky (2006)	47.94	0.35	59.37
	5/7, 5/1, 5/4*3/4	Sultan *et al.* (1986)	40.26	0.2815	52.47
	PC3 PC2 PC1	*e.g.* Chavez *et al.* (1991); Yesou *et al.* (1993)	52.41	0.4095	66.28
Landsat 8	753	742 ETM+, Gad and Kusky (2006)	42.13	0.2885	55.15
	4/6 4/2 6/7	3/5 3/1 7/5 TM, Sabbins (1999)	47.8	0.348	63.16
	2/3 4/5 6/7	This work	46.97	0.34	55.18
	PC3 PC2 PC1	*e.g.* Chavez *et al.* (1991); Yesou *et al.* (1993)	50.99	0.38	59.62
ASTER	3/2 4/1 4/6	Xu *et al.* (2004)	41.34	0.2805	54.83
	4/2 4/5 5/6	Velosky *et al.* (2003)	32.87	0.1727	45.94
	4/6 4/7 3/1	Di Tomasso and Rubinstein (2007)	35.08	0.1956	41.36
	PC3 PC2 PC1	*e.g.* Yujun *et al.* (2007), Gabr *et al.* (2010), Pour and Hashim (2011)	56.27	0.4399	64.8

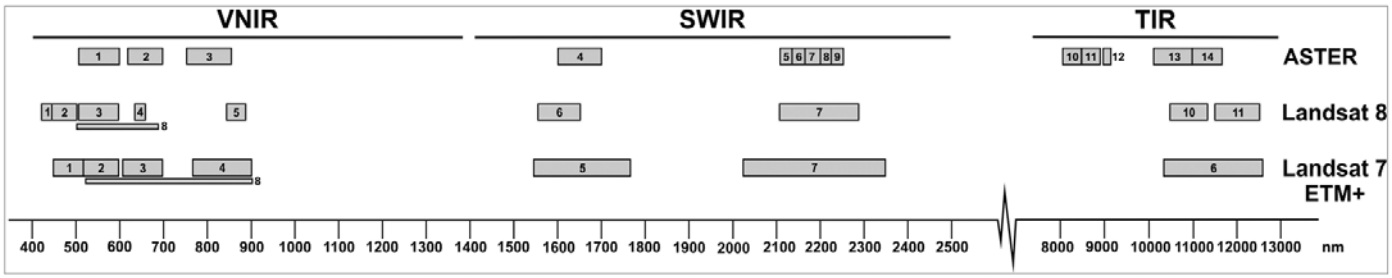

Figure 3: Bandpasses of Landsat 7 ETM+, Landsat 8 and ASTER multispectral sensors.

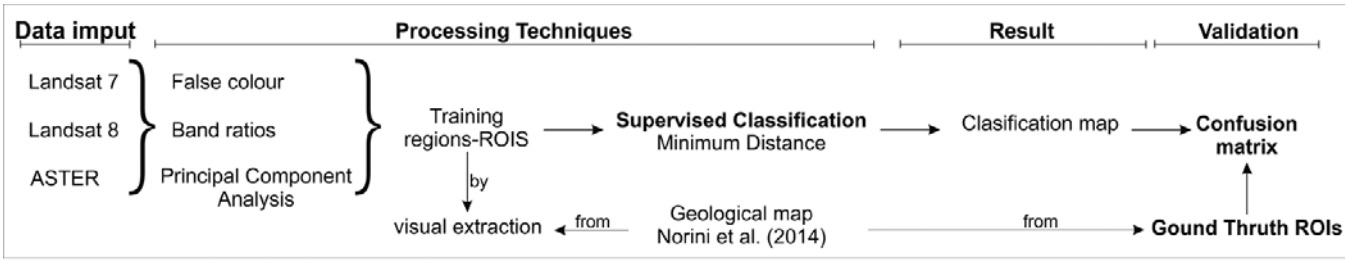

Figure 4: Flow diagram of the research procedure.

corresponding to the lithological units defined by Norini *et al.* (2014) (Fig. 2) (Table 1) were extracted for visual comparison. These training regions were used as inputs to perform the supervised classifications (minimum distance) on the different images (results can be seen in Figs. 5 and 6) obtaining a classification map. This classification uses the mean vector for each class and calculates the Euclidean distance from each unknown pixel to the mean for each class; so the pixels are classified to the nearest class.

Then, an assessment of the classification was produced for every image. A quantitative comparison between the geological map (ground truth) and the results of each classification has been performed to evaluate the capability of these standard processing techniques to reliably depict the geology of the volcano (Fig. 4). There are a number of ways to investigate the accuracy/error in spatial data: visual inspection; non-site specific analysis; difference image creation; error budgeting; and quantitative accuracy assessment (Congalton 2001). The quantitative accuracy of the classifications applied to the different data sets was assessed by comparing the classification with ground truth data (reference data) extracted from the geological map (Norini *et al.* 2014). A confusion matrix (Congalton 1991), and related statistics, was used as accuracy assessing paradigm (Fig. 4). An error matrix is a very effective way to represent accuracy in that the accuracies of each category are plainly described along with both the errors of inclusion (commission errors) and errors of exclusion (omission errors) present in the classification (Congalton 2001). Quantitative accuracy assessment provides a very powerful mechanism for descriptive and analytical evaluation of the spatial data (Congalton 2001). The accuracy of a classification is estimated by comparing a classification outcome with ground truth information by means of a confusion matrix. On the base of the error matrix overall, related statistics coefficients (accuracy and kappa) for each classification image were calculated (Table 2).

RESULTS

From each processed image a classification map was generated by means of supervised classification (minimum distance) (Fig. 4). Ground truth ROIs were extracted from the geological map in order to evaluate the classification results. It's worthy to distinguish that Tuzgle synthem was separated in two units: Old Tuzgle and New Tuzgle since its different spectral response in all the processing techniques. The most recent lava (New Tuzgle) has not alteration, so it looks different in remote sensing data (Fig. 5).

For each classified image, an error matrix was generated to examine and display errors (Annex 1). The related statistics show that principal component analysis have the better results for Landsat 7 (52.41% overall accuracy, 0.41 kappa coefficient), Landsat 8 (50.99% overall accuracy, 0.38 kappa coefficient) and ASTER (56.27% overall accuracy, 0.44 kappa coefficient) classifications over the band ratios and false color composite images (Table 2). Figure 5 illustrates the classification outcomes for all the processing techniques over ASTER data. Classification maps derived from band ratios performed over ASTER data (Fig. 5a, b, c) show lower values of overall accuracy than those obtained from principal component analysis (Fig. 5d) because the classification is not very effective identifying the different classes. The classification result from principal component analysis images most closely resembles to the geological map (Fig. 2) and the bar diagram which compares the ground truth and classified area (Fig. 5d) showing similarities between both. Figure 6 shows the comparison between principal component analysis for the three sensors utilized, since principal component analysis derived classification maps show the highest overall accuracy values (>50 %) and kappa coefficient. New Tuzgle is well classified in the three images because it is the most recent, while the older Basal Dome Complex and Azufre Synthems are misclassified (see bar diagrams in Fig. 6). Among the different principal component analysis, ASTER data have the best results by enable the better accurate classification.

From confusion matrix different errors in the classification maps were extracted. Error of commission shows incorrectly classified samples, while error of omission refers to the relation between the classification classes with the ground truth (Fig. 7). Azufre and Basal Dome Complex are the classes worse classified with the highest values of both errors. New Tuzgle and San Antonio classes have the lowest values of error of omission, while all other classes have relatively high values. Noteworthy, Tuzgle Ignimbrite, Basal Dome Complex and Azufre classes have high values of omission, due to part of the area corresponding to these classes was classified as other category.

In addition, an average of omission and

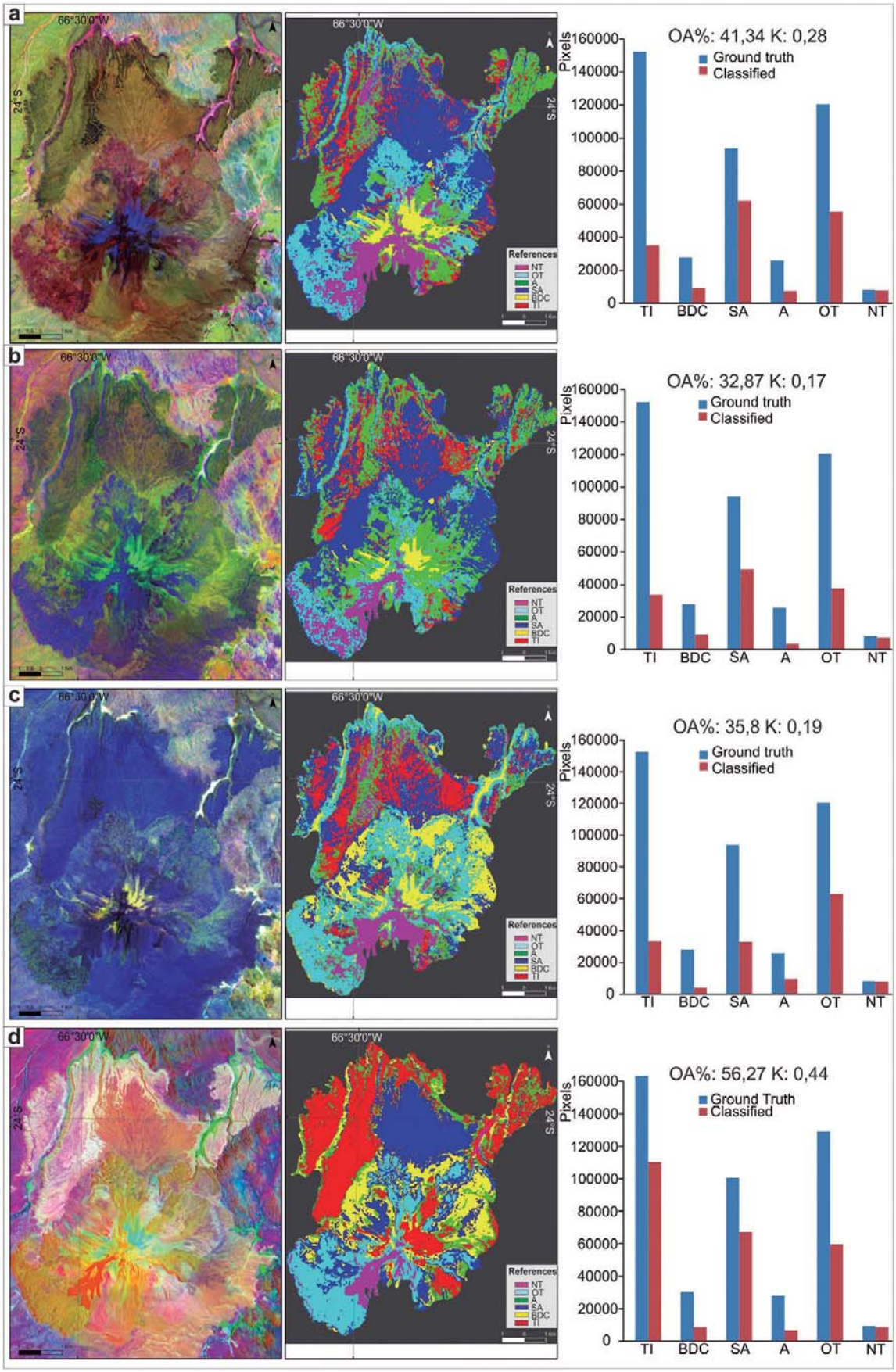

Figure 5: Example of processing techniques on ASTER data. a) RGB 3/2, 4/1, 4/6 over ASTER data (left). Resulting classification map (centre). Bar diagram showing the comparison between ground truth area and classified area for each synthem (right); b) RGB 4/2 4/5 5/6 over ASTER data (left). Resulting classification map (centre). Bar diagram showing the comparison between ground truth area and classified area for each synthem (right); c) RGB 4/6 4/7 3/1 over ASTER data (left). Resulting classification map (centre). Bar diagram showing the comparison between ground truth area and classified area for each synthem (right); d) RGB PC3 PC2 PC1 over ASTER data (left). Resulting classification map (centre). Bar diagram showing the comparison between ground truth area and classified area for each synthem (right). References: OA%: Overall accuracy. K: kappa coefficient. NT: New Tuzgle, OT: Old Tuzgle, A: Azufre, SA: San Antonio; BDC: Basal Dome Complex, TI: Tuzgle Ignimbrite.

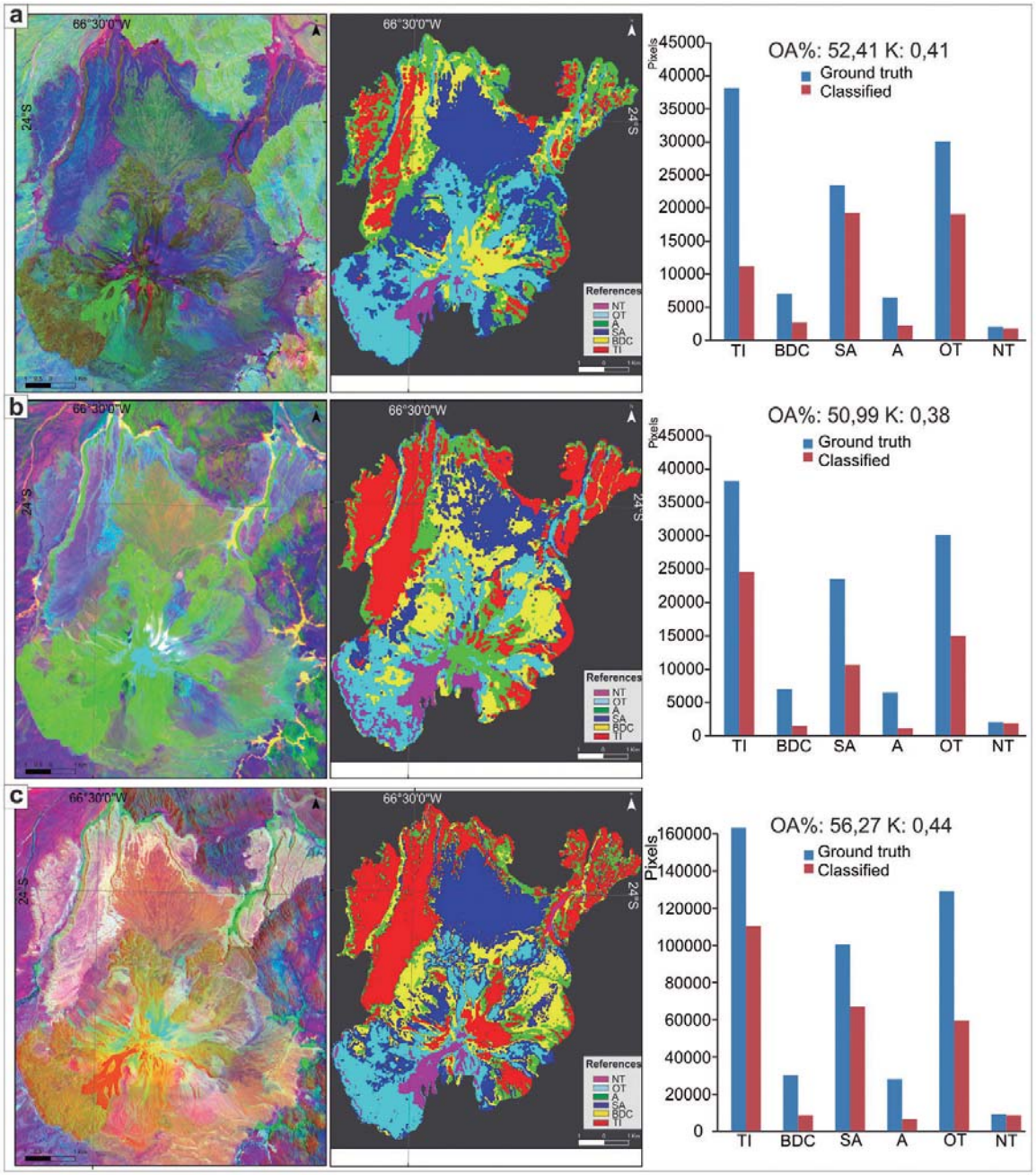

Figure 6: a) RGB PC3 PC2 PC1 over Landsat 7 data (left). Resulting classification map (centre). Bar diagram showing the comparison between ground truth area and classified area for each synthem (right); b) RGB PC3 PC2 PC1 over Landsat 8 data (left). Resulting classification map (centre). Bar diagram showing the comparison between ground truth area and classified area for each synthem (right). c) RGB PC3 PC2 PC1 over ASTER data (left). Resulting classification map (centre). Bar diagram showing the comparison between ground truth area and classified area for each synthem (right).

commission errors of all the classification maps distinguished by class has been performed (Fig. 8). Omission diagrams show low values in San Antonio, Old Tuzgle and New Tuzgle classes (Figs. 8c, e, f). The other classes show moderate values of omission error. From commission diagrams can be seen that Tuzgle Ignimbrite, San Antonio and Old Tuzgle classes are the best classified (Fig. 8a, c, e). Basal Dome Complex class is mistaken for Tuzgle Ignimbrite (Fig. 8b) and New Tuzgle class is confused with Old Tuzgle one (Fig. 8f). Azufre class is the worst classified: in fact it is categorized as Tuzgle Ignimbrite, San Antonio, Old Tuzgle and Basal Dome Complex classes (Fig. 8d). In conclusion, Basal Dome Complex and Azufre synthems are the classes worst classified (Figs. 8b, d). On the other hand, San Antonio, Old Tuzgle and New Tuzgle are the groups best categorized (Figs. 8c, f).

DISCUSSION

Multispectral images were processed in order to test the processing techniques potential for lithological mapping of a volcanic area in an isolated region. The extremely arid conditions of this region and minimal vegetation are encouraging for using optical remote sensing procedures for a preliminary lithological mapping. Tuzgle volcano was chosen since the geology is well known and also be-

cause the volcanics have a huge compositional and textural variation.

Different processing techniques over Landsat 7, 8 and ASTER images were tested and the best results are shown in this work. Since the validation over several processing techniques, we found that supervised classification over PCA in multispectral data was the best methodology for lithological mapping, as can be seen in the overall accuracy values (Table 2, Fig. 6).

Principal component images are useful for reducing data dimensionality, condensing topographic and spectral information, improving image color presentation and enhancing specific spectral features (Liu and Mason 2009). Principal component images are scene dependent and frequently have no obvious correlation with physically interpretable concepts in the same way that band ratios. By visual inspection, it can be seen that principal component analysis images displayed in RGB enabled the best discrimination between units and the boundaries between them are sharper. Principal component analysis has been used as a methodology for hydrothermal alteration recognition by means of Crosta method (Crosta and Moore 1989, Loughlin 1991, Crosta *et al.* 2003) to identify the diagnostic features of hydroxyl-minerals, carbonate-minerals and iron oxides (*e.g.* Tangestani and Moore 2001, Crosta *et al.* 2003, Kargi 2007, Moore *et al.* 2008, Tangestani *et al.* 2008, Pour and Hashim 2011). Also principal component analysis have been used for lithologic mapping, revision of lithological boundaries and characterizing new lithological units in different arid areas (*e.g.* Namibia, Gomez *et al.* 2005; SW Iran, Tangestani 2006; Central-Eastern Desert of Egypt, Amer *et al.* 2010). Supervised classification of principal component bands had be used for digital soil mapping (Boettinger *et al.* 2008).Principal component vectors are scene dependent and frequently have no obvious correlation with physically interpretable concepts (*e.g.* Schott *et al.* 2007). However, based on all classification maps resulting of remote sensing analysis

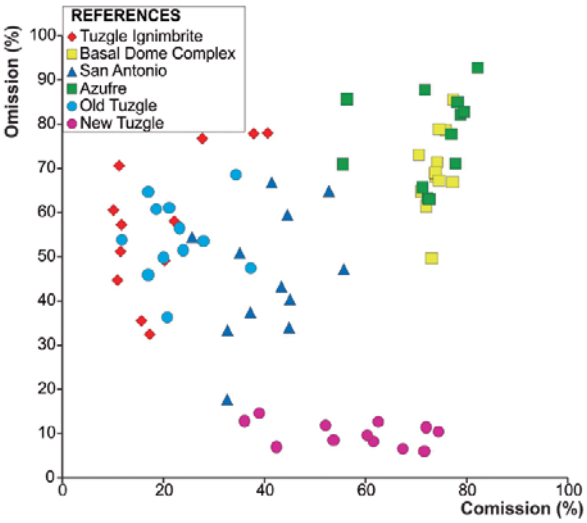

Figure 7: Scatter diagram showing comission (%) and omission (%) for all the processing techniques for all the Tuzgle volcano synthems.

from Tuzgle Volcano, principal component analysis derived classifications show the best results being the most powerful methodology for lithological mapping. This is possible since the principal components bands produce more colorful color composite images than spectral color composite images because the data is uncorrelated (Liu and Mason 2009), so the differences between materials becomes more evident. So we propose classified map derived from principal component analysis on multispectral satellite data for volcanic lithological mapping in arid environments. Comparing the three multispectral sensors used in this work, we achieve better results and more accuracy with ASTER images. This is expected as ASTER data have wide spectral coverage in the visible near-infrared through short-wave infrared to the thermal infrared regions (Fig. 3) and high spatial resolution.

By a close interpretation of the results of the supervised classification we can observe that Tuzgle Ignimbrite and Basal Dome Complex classes are confused with each other (Figs. 8a, b). The reason for this misclassification is due to both classes have the same geochemical composition. To check the impact of this phenomenon in the classification outcome, a new confusion matrix that merges these two classes in a new one was performed and a new value of overall accuracy was calculated (overall accuracy*, Table 2). These overall accuracies* show an important improvement of 12% approximately respect to the originals. Compositions are limitations of this methodology due to the similar spectral response. However these two units have very different texture since its nature: a pyroclastic flow and lava domes. In these case, high spatial resolution images (*e.g.* Spot, Ikonos), available for free on Google Earth platform for viewing, become a powerful tool to check rocks with similar composition but different textures, morphology and outcrop pattern improving and complementing the results of the classification.

There are no generally accepted limits on how accurate a classification should be, but usually a 70% of overall accuracy for each class is considered acceptable (Foody 2002, Thomlinson *et al.* 1999, Smits *et al.* 1999). From supervised classification findings derived from Principal Component Analysis, which shown the best accuracies, overall accuracies for each class were computed (Table 3). Tuzgle Ignimbrite, San Antonio and Old Tuzgle classes are truthfully classified. The low values founded in Basal Dome Complex class (Table 3) are due to the similar geochemical composition between this class and Tuzgle Ignimbrite. Azufre Synthem is classified wrongly (9.54% average overall accuracy) because these rocks are affected by hydrothermal alteration, and present snow cover and high slope. These

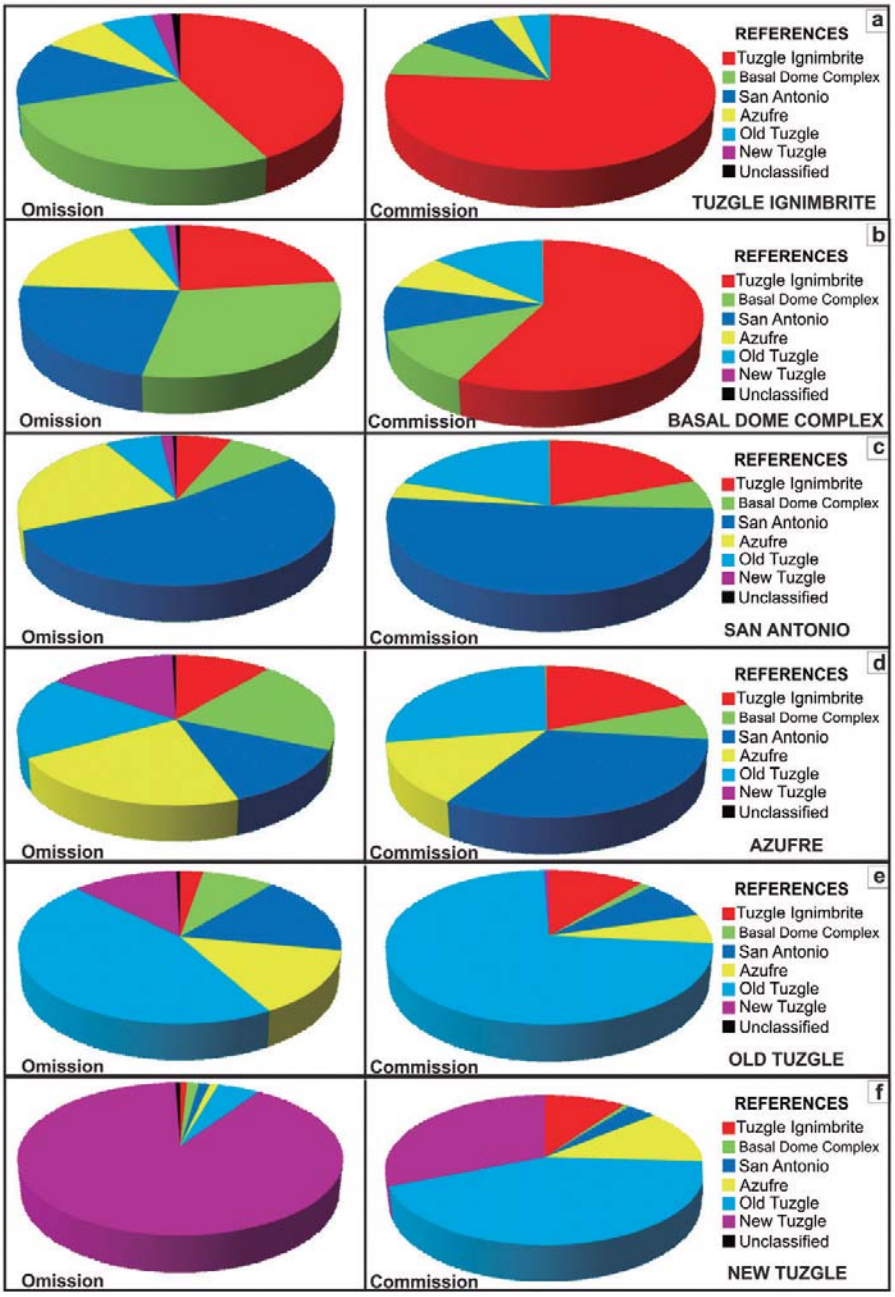

Figure 8: Omission and commission diagrams for: a) Tuzgle Ignimbrite; b) Basal Dome Complex; c) San Antonio; d) Azufre; e) Old Tuzgle; f) New Tuzgle.

TABLE 3: Overall accuracy by class for supervised classification over PCA images for Landsat 7, Landsat 8 and ASTER.

	Overall Accuracy					
	Ti	Bdc	Sa	A	Ot	Nt
CPA ASTER	79.35%	15.78%	60.97%	8.29%	85.92%	49.53%
CPA LANDSAT 7	86.56%	14.05%	61.05%	15.09%	75.29%	53.52%
CPA LANDSAT 8	81.3%	11.01%	69.31%	5.24%	76.03%	26.66%
Averagevalue	82.4%	13.61%	63.78%	9.54%	79.08%	43.24%

factors are the principal problems in classification of optical imagery applied to composite volcanoes. Finally, New and Old Tuzgle classes correspond to the same synthem (Table 1, Tuzgle Synthem). By means of the visual inspection of the images, this synthem was divided in two classes because of the spectral differences between the old and new lavas due to the different degree of alteration. New Tuzgle class has moderate values of overall accuracy, since in this class the pixels are classified principally like Old Tuzgle class. This is because both classes have the same composition and they are part of the same synthem.

CONCLUDING REMARKS

Mapping on volcanic regions is indispensable for determine the rock types that have been erupted, their spatial distribution and stratigraphic relationships for the assessment of the geologic hazard and the exploration of mineral resources. The peculiar conditions of Puna Plateau (aridity, lack of vegetation, altitude) make the optical processing techniques very useful for lithological mapping. Many of the volcanoes located at the Puna Plateau are difficult to access or inaccessible so an effective remote sensing methodology for preliminary geological mapping becomes necessary.

In the current study, we found that supervised classification over principal component analysis images derived from multispectral data is the best practical and efficient methodology for preliminary lithological mapping. The results show that even for unknown arid regions considerable amount of information can be extracted from Landsat 7, 8 and ASTER multispectral data.

The low costs, data availability and broad swath of the multispectral data, make them valuable for lithological mapping in the Puna Plateau region, despite some problems can be found (hydrothermal alteration, snow cover, and steep areas). Multispectral satellite remote sensing methods are a powerful tool for detailed geologic analysis, especially in difficult to access or inaccessible and/or large non-vegetated as Puna Plateau.

We suggest that these techniques may be used as time- and cost-effective approach

for preliminary lithological mapping in volcanic arid areas. Even if this methodology is very useful to composite volcano preliminary mapping, the correct reconstruction of the stratigraphy of a volcano always requires field survey.

ACKNOWLEDGEMENTS

The images used in this work are courtesy of United States Geological Survey. This work was supported by CNR-Curiosity driven 2008 grant (Italy) to Gianluca Groppelli, SAOCOM N° 40 project (CONAE-Argentina) to José Germán Viramonte and CIUNS a N° 1978/1 grant (Argentina) to Marcelo Arnosio. The authors would like to thank the reviewers for their valuable comments which gave the opportunity to improve the manuscript significantly.

WORKS CITED IN TEXT

Abdeen, M.M., Allison, T.K., Abdelsalam, M.G. y Stern, R.J. 2001. Application of ASTER band-ratio images for geological mapping in arid regions; the Neoproterozoic Allaqi Suture, Egypt. Geological Society of America Annual Meeting, Abstracts 3:289, Boston.

Abdelsalam, M.G. y Stern, R.J. 1996. Sutures and shear zones in the Arabian Nubian Shields. Journal of African Earth Sciences 23: 289-310.

Aboelkhair, H., Ninomiya, Y., Watanabe, Y. y Sato, I. 2010. Processing and interpretation of ASTER TIR data for mapping of rare-metal-enriched albitegranitoids in the Central Eastern Desert of Egypt. Journal of African Earth Sciences 58: 141-151.

Abrams, J.M., Brown, D., Lepley, L. y Sadowski, R. 1983. Remote sensing for porphyry copper deposits in Southern Arizona. Economic Geology 78: 591-604.

Acocella, V., Gioncada, A., Omarini, R., Riller, U., Mazzuoli, R. y Vezzoli, L. 2011. Tectonomagmatic characteristics of the back-arc portion of the Calama–Olacapato–El Toro Fault Zone, Central Andes.Tectonics 30,TC3005, doi:10.1029/2010TC002854.

Allmendinger, R., Ramos, V., Jordan, T., Palma, M. y Isacks, B. 1983. Paleogeography and Andean structural geometry, Northwest Argentina. Tectonics 2: 1-16.

Allmendinger, R.W., Jordan, T.E., Kay, S.M. e Isacks, B.L. 1997. The evolution of the Altiplano-Puna Plateau of the Central Andes. Annual Review Earth Planetary Sciences 25: 139-174.

Amer, R., Kusky, T. y Ghulam, A. 2010. Lithological mapping in the Central Eastern Desert of Egypt using ASTER data. Journal of African Earth Sciences 56: 75-82.

ANCORP Working Group 2003.Seismic imaging of a convergent continental margin and plateau in the central Andes (Andean Continental Research Project 1996-ANCORP'96). Journal of Geophysical Research, Solid Earth 108: 1978-2012.

Assiri, A., Alsaleh A. y Mousa, H. 2008. Exploration of hydrothermal alteration zones using ASTER imagery: A case study of Nuqrah area, Saudi Arabia. Asian Journal Earth Sciences 1: 77-82.

Bhatti, S.S. y Tripathi, N.K. 2014.Built-up area extraction using Landsat 8 OLI imagery. GIScience & Remote Sensing 51: 445-467.

Boettinger, J.L., Ramsey R.D., Bodily, J.M. Cole, N.J. Kienast-Brown S., Nield S.J., Saunders A.M. y Stum. A.K. 2008.Landsat Spectral Data for Digital Soil Mapping. En: Hartemink, A.E.,McBratney, A.B. yMendonça-Santos, M. (eds.), Digital Soil Mapping with Limited Data, Springer: 193-202, Amsterdam.

Chavez, P.S., Sides, S.C. y Anderson, J.A. 1991. Comparison of 3 different methods to merge multiresolution and multispectral data-Landsat TM and SPOT panchromatic. Photogrammetric Engineering and Remote Sensing 57: 295-303.

Cogliati, S. 2011. Analisimorfostrutturale, stratigrafica e petrografica del Vulcano Tuzgle (Argentina). MSc Thesis Università degli Studi di Milano (Unpublished), 148 p., Milano.

Coira, B. y Kay, S. M. 1993. Implications of Quaternary volcanism at Cerro Tuzgle for crustal and mantle evolution of the Puna Plateau, Central Andes, Argentina. Contributions to Mineralogy and Petrology 113: 40-58.

Congalton, R.G. 2001.Accuracy assessment and validation of remotely sensed and other spatial information. International Journal of Wildland Fire 10: 321-328.

Congalton, R.G. 1991. A review of assessing the accuracy of classifications of remotely sensed data. Remote Sensing of Environment 37: 35-46.

Crosta, A.P. y Moore, J.McM. 1989. Enhancement of Landsat Thematic Mapper imagery for residual soil mapping in SW Minas Gerais State Brazil: a prospecting case history in greenstone belt terrain. Proceedings of the 9th Thematic Conference on Remote Sensing for Exploration Geology, 1173-1187, Calgary.

Crosta, A.P., Souza Filho, C.R., Azevedo, F. y Brodie, C. 2003. Targeting key alteration minerals in epithermal deposits in Patagonia, Argentina, using ASTER imagery and principal component analysis. International Journal of Remote Sensing 24: 4233–4240.

de Silva, S.L. y Francis P.W. 1991. Volcanoes of the Central Andes. Springer-Verlag, 213 p., New York.

Deruelle, B. 1982.Petrology of the plio-quaternary volcanism of the South-Central and Meridional Andes. Journal of Volcanology and Geothermal Research 14: 77-124.

Di Tommaso, I. y Rubinstein, N. 2007. Hydrothermal alteration mapping using ASTER data in the Infiernillo porphyry deposit, Argentina. Ore Geology Reviews 32: 275-290.

Fernandes, R., Butson, C., Leblanc, S. y Latifovic, R. 2003. Landsat-5 TM and Landsat-7 ETM+ based accuracy assessment of leaf area index products for Canada derived from SPOT-4 VEGETATION data. Canadian Journal of Remote Sensing 29: 241-258.

Foody, G.M. 2002.Status of land cover classification accuracy assessment. Remote Sensing of Environment 80: 185-201.

Gabr, S., Ghulam, A. y Kusky, T. 2010.Detecting areas of high-potential gold mineralization using ASTER data. Ore Geology Reviews 38: 59-69.

Gad, S. y Kusky, T. 2006. Lithological mapping in the Eastern Desert of Egypt, the Barramiya area, using Landsat thematic mapper (TM). Journal of African Earth Sciences 44: 196-202.

Gomez, C., Delacourt, C., Allemand, P., Ledru, P. y Wackerle, R. 2005. Using ASTER remote sensing data set for geological mapping, in Namibia. Physics and Chemistry of the Earth 30: 97-108.

González-Ferrán, O. 1995.Volcanes de Chile. Instituto Geográfico Militar, 640 p., Santiago.

Gutpa, R.P. 2003. Remote Sensing Geology, Second edition. Springer-Verlag, 656 p., Berlin.

Hubbard, B.E., Crowley, J.K. y Zimbelman, D.R. 2003. Comparative alteration mineral mapping using visible to shortwave infrared (0.4–2.4 m) Hyperion, ALI, and ASTER imagery. IEEE Transactions on Geoscience and Remote Sensing 41: 1401-1410.

Hunt G.R. y Vincent R.K. 1968. The behaviour of spectral features in the infrared emission from particulate surfaces of various grain sizes. Journal of Geophysical Research 73: 6039-6046.

Hunt G.R., Salisbury J.W. y Lehnoff, C.J. 1971. Visible and near infrared spectral of minerals and rocks: III. Oxides and Oxyhydroxides. Modern Geology 2: 195-205.

Jensen, J.R. 2002. Remote Sensing of the Enviroment: An Earth Resource Perspective, Prentice Hall International Limited, 483 p., London.

Kargi, H. 2007. Principal components analysis for borate mapping. International Journal of Remote Sensing 28: 1805-1817.

Kay, S.M. y Coira, B.L. 2009. Shallowing and steepening subduction zones, continental lithospheric loss, magmatism, and crustal-flow under the Central Andean Altiplano–Puna Plateau. En: Kay, S.M. (ed.), Backbone of the Americas: Shallow Subduction, Plateau Uplift, and Ridge and Terrane Collision, Geological Society of America Memoir: 229-259, Denver.

Liu, J.G. y Mason P.J. 2009. Essential Image Processing and GIS for Remote Sensing. John Wiley & Sons Ltd., 443 p., Oxford.

Loughlin, W.P. 1991. Principal Component Analysis for alteration mapping. Photogrammetric Engineering and Remote Sensing 57: 1163-1169.

Lyon, R. J. P. 1965. Analysis of rocks by spectral infrared emission (8 to 25 microns). Economic Geology 60: 715-736.

Matteini, M., Mazzuoli, R., Omarini, R., Cas, R. y Maas, R. 2002. The geochemical variations of the upper cenozoic volcanism along the Calama-Olacapato-Toro transversal fault system in Central Andes (~24ºS): petrogenetic and geodynamic implications. Tectonophysics 345: 211-227.

Mazzuoli, R., Vezzoli, L., Omarini, R., Acocella, V., Gioncada, A., Matteini, M., Dini, A., Guillou, H., Hauser, N., Uttini, A. y Scaillet, S. 2008. Miocene magmatism and tectonics of the easternmost sector of the Calama–Olacapato–El Toro fault system in Central Andes at 24°S: insights into the evolution of the Eastern Cordillera. Geological Society of America Bulletin 120: 1493-1517.

Moghtaderi, A., Moore, F. y Mohammadzadeh, A. 2007. The application of advanced spaceborne thermal emission and reflection (ASTER) radiometer data in the detection of alteration in the Chadormalu paleocrater, Bafq region, Central Iran. Journal of Asian Earth Sciences 30: 238-252.

Moore, F., Rastmanesh, F., Asady, H. y Modabberi, S. 2008. Mapping mineralogical alteration using principal component analysis and matched filter processing in Takab area, north-west Iran, from ASTER data. International Journal of Remote Sensing 29: 2851-2867.

Ninomiya, Y. y Fu, B. 2002. Mapping quartz, carbonate minerals and mafic–ultramafic rocks using remotely sensed multispectral thermal infrared ASTER data. Aero Sense 2002, International Society for Optics and Photonics: 191-202.

Norini G., Báez W., Becchio R., Viramonte J., Giordano G., Arnosio M., Pinton A. y Groppelli G. 2013. The Calama–Olacapato–El Toro fault system in the Puna Plateau, Central Andes: Geodynamic implications and strato volcanoes emplacement. Tectonophysics 608: 1280-1297.

Norini G., Cogliati S., Baez W., Arnosio M., Bustos E., Viramonte J. y Groppelli G. 2014. The geological and structural evolution of the Cerro Tuzgle Quaternary stratovolcano in the back-arc region of the Central Andes, Argentina. Journal of Volcanology and Geothermal Research 285: 214-228.

Papp, É. y Cudahy T. 2002. Hyperspectral remote sensing. Geophysical and Remote Sensing Methods for Regolith Exploration 144: 13-21.

Petrinovic, I.A., Riller, U., Brod, A., Alvarado, D. y Arnosio, M. 2006. Bimodal volcanism in a tectonic transfer zone: evidence for a tectonically controlled magmatism in the Southern Central Andes, NW Argentina. Journal of Volcanology and Geothermal Research 152: 240-252.

Pour, B.A. y Hashim, M. 2011. Spectral transformation of ASTER data and the discrimination of hydrothermal alteration minerals in a semi-arid region, SE Iran. International Journal of the Physical Sciences 6: 2037-2059.

Qari M., Madani A., Matsah M. y Hamimi Z. 2008. Utilization of Aster and Landsat data in geologic mapping of basement rocks of Arafat Area, Saudi Arabia. The Arabian Journal for Science and Engineering 33: 99-116.

Ramelow, J., Riller, U., Romer, R.L. y Oncken, O. 2006. Kinematic link between episodic trapdoor collapse of the Negra Muerta Caldera and motion on the Olacapato-El Toro Fault Zone, southern central Andes. International Journal of Earth Sciences 95: 529-541.

Riller, U., Petrinovic, I., Ramelow, J., Strecker, M. y Oncken, O. 2001.Late Cenozoic tectonism, caldera and plateau formation in the Central Andes. Earth Planetary Science Letters 188: 299-311.

Rowan, L.C. y Mars J.C. 2003.Lithologic mapping in the Mountain Pass, California, area using Advanced Spaceborne Emission and Reflection Radiometer (ASTER) data. Remote Sensing of Environment 84: 350-366.

Rowan, L.C., Hook, S.J., Abrams, M.J. y Mars, J.C. 2003. Mapping hydrothermally altered rocks at Cuprite, Nevada, using the Advanced Spaceborne Thermal Emission and Reflection Radiometer (ASTER), a new satellite-imaging system. Economic Geology 98: 1019-1027.

Roy, D.P., Wulder, M.A., Loveland, T.R., Allen, R.G., Anderson, M.C., Helder, D. y Zhu, Z. 2014. Landsat-8: Science and product vision for terrestrial global change research.Remote Sensing of Environment145: 154-172.

Sabins, F.F., 1999. Remote sensing for mineral exploration. Ore Geology Reviews 14: 157-183.

Salfity, J. 1985. Lineamientos transversales al rumbo andino en el noroeste argentino. 4º Congreso Geológico Chileno, Actas 2: 119-137, Antofagasta.

Schott J.R. 2007. Remote Sensing: The Image Chain Approach, 2nd edition. Oxford University Press, 666 p., New York.

Schwab, K. y Lippolt, H. 1974. K-Ar mineral ages and late Cenozoic history of the Salar de Cauchari area (Argentine Puna). En: Gonzales-Ferrán, O. (ed.), Proceedings of the Symposium on Andean and Antarctic Volcanology Problems, International Association of Volcanology and Chemistry of the Earth's Interior Special Series: 697-714, Roma.

Smits, P.C., Dellepiane, S.G. y Schowengerdt,

R.A. 1999. Quality assessment of image classification algorithms for land-cover mapping: A review and a proposal for a cost-based approach. International Journal of Remote Sensing 20: 1461-1486.

Son, Y. S., Kang, M. K. y Yoon, W. J. 2014. Pyrophyllite mapping in the Nohwa deposit, Korea, using ASTER remote sensing data.Geosciences Journal18: 295-305.

Sultan, M., Arvidson, R.E. y Sturchio, N.C. 1986.Mapping of serpentinites in the Eastern Desert of Egypt by using Landsat thematic mapper data. Geology 14: 995-999.

Tangestani, M.H. 2006.A comparative approach on TIR and VNIR-SWIR datasets of ASTER instrument for lithological mapping at the Neyrizophiolite zone, SW Iran. Proceedings of Map Asia 2006: 29, Bangkok.

Tangestani, M.H. y Moore, F. 2001. Comparison of three principal component analysis techniques to porphyry copper alteration mapping: a case study, Meiduk area, Kerman, Iran. Canadian Journal of Remote Sensing 27: 176-181.

Tangestani, M.H., Mazhari, N., Ager, B. y Moore, F. 2008. Evaluating advance spaceborne thermal emission and reflection radiometer (ASTER) data for alteration zone enhancement in a semi-arid area, northern shahr-e-Babak, SE Iran. International Journal of Remote Sensing 29: 2833-2850.

Thomlinson, J.R., Bolstad, P.V. y Cohen, W.B. 1999. Coordinating methodologies for scaling landcover classifications from site-specific to global: Steps toward validating global map products. Remote Sensing of Environment 70: 16-28.

Trumbull, R., Riller, U., Oncken, O., Scheuber, E., Munier, K. y Hongn, F. 2006. The time-space distribution of Cenozoic volcanism in the South-Central Andes: a new data compilation and some tectonic implications. En: Oncken, O., Chong, G., Franz, G., Giese, P., Götze, H., Ramos, V., Strecker, M. y Wigger, P. (eds.) The Andes - Active Subduction Orogeny, Springer: 29-43, Berlin.

Van der Meer, F. D., van der Werff, H., van Ruitenbeek, F. J., Hecker, C. A., Bakker, W. H., Noomen, M. F. y Woldai, T. 2012. Multi-and hyperspectral geologic remote sensing: A review.International Journal of Applied Earth Observation and Geoinformation14: 112-128.

Velosky, J.C., Stern, R.J. y Johnson, P.R. 2003. Geological control of massive sulfide mineralization in the Neoproterozoic Wadi Bidah shear zone, southwestern Saudi Arabia, inferences from orbital remote sensing and field studies. Precambrian Research 123: 235-247.

Viramonte J.G. y Petrinovic I. 1990. Cryptic and parially buried calderas along strike slipe fault system in the Central Andes. International Symposium on Andean Geodynamic, Actas I: 318-320, Grenoble.

Viramonte, J.G., Galliski, M.A., Araña Saavedra, V., Aparício, A., García Cucho, L. y Martín Escorza, C. 1984. El finivulcanismo básico de la depresión de Arizaro, provincia de Salta. 9º Congreso Geológico Argentino, Actas 3: 234-251, Bariloche.

Watanabe, H. y Matsuo K. 2003. Rock type classification by multi-band TIR of ASTER. Geosciences Journal7: 347-358.

Xu, Y., Qizhong, L., Yun, S. y Lu, W. 2004. Extraction mechanism of alteration zones using ASTER imagery. Geosciences and Remote Sensing Symposium, Actas 6: 4174-4175, Texsas..

Yamaguchi, Y., Kahle, A.B., Tsu, H., Kawakami, T. y Pniel, M. 1998. Overview of advanced spaceborne thermal emission and reflection radiometer (ASTER).Geoscience and Remote Sensing 36: 1062-1071.

Yesou, H., Besnus, Y., Rolet, J. 1993. Extraction of spectral information from LandsatTM data and merger with SPOT panchromatic imagery - a contribution to the study of geological structures. Journal of Photogrammetry and Remote Sensing 48: 23-36.

Yuan, X., Sobolev, S. V., Kind, R., Oncken, O., Bock G., Asch, G., Schurr, B., Graeber, F., Rudloff, A., Hanka, W., Wylegalla, K., Tibi, R., Haberland, Ch., Rietbrock, A., Giese, P., Wigger, P., Röwer, P., Zandt, G., Beck, S., Wallace, T., Pardo, M. y Comte, D. 2000. Subduction and collision processes in the Central Andes constrained by converted seismic phases. Nature 408: 958-961.

Yujun, Z., Jianmin, Y., Fojun, Y. 2007. The potentials of multi-spectral remote sensing techniques for mineral prognostication—taking Mongolian Oyu Tolgoi Cu–Au deposit as an example. Earth Science Frontiers 14: 63-70.

Recibido: 22 de marzo, 2016
Aceptado: 27 de marzo, 2017

Annex I: Confusion matrixes

Confusion matrixes for every image are shown. References: TI: Tuzgle Ignimbrite; BDC: Basal Dome Complex; SA: San Antonio; A: Azufre; OT: Old Tuzgle and NW: New Tuzgle.

Confusion Matrix for Landsat 7.

RGB 5/3 5/1 5/7

		Ground Truth						
		Tuzgle Ignimbrite	Basal Dome Complex	San Antonio	Azufre	Old Tuzgle	New Tuzgle	Total
Classification	unclassified	259	34	82	15	121	26	537
	TI	15015	1083	392	356	196	40	17082
	BDC	12314	1998	1675	623	829	32	17471
	SA	5070	3272	13990	1571	6332	28	30263
	A	3167	493	5533	960	3803	37	13993
	OT	962	23	1101	1178	11703	72	15039
	NT	1408	103	714	1780	7116	1824	12945
	Total	38195	7006	23487	6483	30100	2059	107330

RGB 7/5 5/4 3/1

		Ground Truth						
		Tuzgle Ignimbrite	Basal Dome Complex	San Antonio	Azufre	Old Tuzgle	New Tuzgle	Total
Classification	unclassified	205	35	42	26	118	21	447
	TI	16271	1532	177	489	432	16	18917
	BDC	10742	1494	1423	1073	1166	88	15986
	SA	7053	1914	13299	622	4617	42	27547
	A	1339	1952	7075	2374	4288	5	17033
	OT	1751	63	1304	925	16220	88	20351
	NT	834	16	167	974	3259	1799	7049
	Total	38195	7006	23487	6483	30100	2059	107330

RGB 5/7 5/1 5/4*3/4

		Ground Truth						
		Tuzgle Ignimbrite	Basal Dome Complex	San Antonio	Azufre	Old Tuzgle	New Tuzgle	Total
Classification	unclassified	349	45	126	26	149	27	722
	TI	18587	1524	563	523	308	53	21558
	BDC	11585	2231	2854	806	1432	35	18943
	SA	2475	2335	7738	823	1918	18	15307
	A	2031	679	9912	1144	5046	15	18827
	OT	1167	60	1345	1295	11668	68	15603
	NT	2002	132	949	1866	9579	1843	16371
	Total	38196	7006	23487	6483	30100	2059	107331

RGB PC 3 PC 2 PC 1

		Ground Truth						
		Tuzgle Ignimbrite	Basal Dome Complex	San Antonio	Azufre	Old Tuzgle	New Tuzgle	Total
Classification	unclassified	176	28	35	9	50	4	302
	TI	11184	1323	34	208	171	0	12920
	BDC	13558	2689	759	825	1292	14	19137
	SA	3156	2035	19324	1134	5888	117	31654
	A	7848	751	1332	2215	2524	11	14681
	OT	2137	179	1850	1944	19087	155	25352
	NT	137	1	153	148	1088	1758	3285
	Total	38196	7006	23487	6483	30100	2059	107331

Confusion Matrixfor Landsat 8.

RGB 753

		Tuzgle Ignimbrite	Basal Dome Complex	San Antonio	Azufre	Old Tuzgle	New Tuzgle	Total
Classification	unclassified	259	34	82	15	121	26	537
	TI	15015	1083	392	356	196	40	17082
	BDC	12314	1998	1675	623	829	32	17471
	SA	5070	3272	13990	1571	6332	28	30263
	A	3167	493	5533	960	3803	37	13993
	OT	962	23	1101	1178	11703	72	15039
	NT	1408	103	714	1780	7116	1824	12945
	Total	38195	7006	23487	6483	30100	2059	107330

RGB 4/6 4/2 6/7

		Ground Truth						
		Tuzgle Ignimbrite	Basal Dome Complex	San Antonio	Azufre	Old Tuzgle	New Tuzgle	Total
Classification	unclassified	660	83	227	51	241	13	1275
	TI	15985	1810	553	1795	1596	1	21740
	BDC	14680	3518	4502	1292	3442	21	27455
	SA	2793	826	14681	344	7748	22	26414
	A	1441	535	1832	780	754	0	5342
	OT	2409	234	1651	1310	14548	187	20339
	NT	254	1	46	911	1778	1822	4812
	Total	38222	7007	23492	6483	30107	2066	107377

RGB 2/3 4/5 6/7

		Ground Truth						
		Tuzgle Ignimbrite	Basal Dome Complex	San Antonio	Azufre	Old Tuzgle	New Tuzgle	Total
Classification	unclassified	1284	95	308	86	411	14	2198
	TI	21080	1729	300	556	579	0	24244
	BDC	7082	2459	1307	2352	2890	18	16108
	SA	2268	416	11512	968	4654	8	19826
	A	4727	1986	7798	458	6748	15	21732
	OT	1497	306	2067	991	13038	121	18020
	NT	284	16	200	1072	1787	1890	5249
	Total	38222	7007	23492	6483	30107	2066	107377

RGB PC3 PC2 PC1

		Ground Truth						
		Tuzgle Ignimbrite	Basal Dome Complex	San Antonio	Azufre	Old Tuzgle	New Tuzgle	Total
Classification	unclassified	325	22	19	12	63	6	447
	TI	24562	2861	650	973	1167	0	30213
	BDC	6414	1470	788	2050	2587	40	13349
	SA	2430	534	10663	462	1289	6	15384
	A	2164	1939	9348	1105	6492	25	21073
	OT	1870	163	1718	897	15034	91	19773
	NT	431	17	301	984	3468	1891	7092
	Total	38196	7006	23487	6483	30100	2059	107331

Confusion Matrix for ASTER.

RGB 3/2 4/1 4/6

		Ground Truth						
		Tuzgle Ignimbrite	Basal Dome Complex	San Antonio	Azufre	Old Tuzgle	New Tuzgle	Total
Classification	unclassified	633	104	226	36	308	38	1345
	TI	35278	5903	9453	489	1520	73	52716
	BDC	51946	9156	6260	5970	9429	98	82859
	SA	36522	8395	61931	4581	21847	32	133308
	A	2526	1264	3477	7459	7123	177	22026
	OT	15751	2140	9051	883	55689	76	83590
	NT	9691	971	3552	6395	24523	7709	52841
	Total	152347	27933	93950	25813	120439	8203	428685

RGB 4/2 4/5 5/6

		Ground Truth						
		Tuzgle Ignimbrite	Basal Dome Complex	San Antonio	Azufre	Old Tuzgle	New Tuzgle	Total
Classification	unclassified	325	39	67	7	200	15	653
	TI	33555	3513	20457	162	3523	6	61216
	BDC	52544	9230	16213	9648	30433	67	118135
	SA	51208	12717	49490	5293	28638	35	147381
	A	1382	334	2086	3647	3495	131	11075
	OT	12442	2063	5465	5714	37578	529	63791
	NT	889	37	172	1342	16572	7420	26432
	Total	152345	27933	93950	25813	120439	8203	428683

RGB 4/6 4/7 3/1

		Ground Truth						
		Tuzgle Ignimbrite	Basal Dome Complex	San Antonio	Azufre	Old Tuzgle	New Tuzgle	Total
Classification	unclassified	350	44	112	29	190	18	743
	TI	33390	2327	27592	456	1050	38	64853
	BDC	24622	4014	6214	3165	13710	207	51932
	SA	43360	5484	32799	1011	5798	21	88473
	A	12832	8838	15503	9493	23375	72	70113
	OT	29345	5782	9761	5437	62999	173	113497
	NT	8447	1445	1969	6222	13316	7674	39073
	Total	152346	27934	93950	25813	120438	8203	428684

RGB PC3 PC2 PC1

		Ground Truth						
		Tuzgle Ignimbrite	Basal Dome Complex	San Antonio	Azufre	Old Tuzgle	New Tuzgle	Total
Classification	unclassified	542	53	170	39	130	3	937
	TI	102614	9415	3230	7404	6557	103	129323
	BDC	27172	7481	4360	3277	5120	0	47410
	SA	6574	3185	62529	3191	27075	8	102562
	A	12946	7636	20640	5698	21741	42	68703
	OT	745	159	2869	4868	55282	413	64336
	NT	1754	4	152	1336	4534	7634	15414
	Total	152347	27933	93950	25813	120439	8203	428685